Nucleus ($22 \leq Z_p \leq 28$)-Nucleus Interactions between 20 and 65 GeV per Nucleon*

T. H. Burnett (h), S. Dake (b), J. H. Derrickson (f), W. F. Fountain (f), M. Fuki (c), J. C. Gregory (g), T. Hayashi (b), T. Hayashi (g,j), R. Holynski (i), J. Iwai (h), W. V. Jones (e), A. Jurak (i), J. J. Lord (h), C. A. Meegan (f), O. Miyamura (d), H. Oda (b,f), T. Ogata (a), T. A. Parnell (f), F. E. Roberts (f), T. Saito (a), T. Tabuki (a), Y. Takahashi (f,g), T. Tominaga (d), J. W. Watts (f), B. Wilczynska (i), R. J. Wilkes (h), W. Wolter (i) and B. Wosiek (i,e).

(a) Institute for Cosmic Ray Research, University of Tokyo, Tokyo 188, Japan; (b) Department of Physics, Kobe University, Kobe 657, Japan; (c) Department of Physics, Okayama University of Science, Okayama 700, Japan; (d) Department of Applied Mathematics, Osaka University, Osaka 560, Japan; (e) Department of Physics and Astronomy, Louisiana State University, Baton Rouge, Louisiana 70803, USA; (f) Space Science Laboratory, NASA/Marshall Space Flight Center, Huntsville, Alabama 35812, USA; (g) School of Science, The University of Alabama in Huntsville, Huntsville, Alabama 35899, USA; (h) Department of Physics, University of Washington, Seattle, Washington 98105, USA; (i) Institute for Nuclear Physics, PL-30-055 Krakow, Poland; (j) Science and Engineering Research Laboratory, Waseda University, Tokyo 162, Japan.

PACS Numbers: 25.70.G, 13.85.T

A hybrid electronic counter-emulsion chamber instrument was exposed to high energy cosmic rays on a balloon. The data on 105 nucleus-nucleus collisions in the energy range 20 to 65 GeV/nucleon and for incident nuclear charges $22 \leq Z_p \leq 28$ are presented. Inclusive characteristics of particle production on different targets (plastic, emulsion and lead) are shown and compared with models based on the superposition of nucleon-nucleus interactions. Features of a subset of the more central collisions with plastic target and some characteristics of individual events with the highest multiplicity of produced particles are described.

1. Introduction

Collisions between heavy nuclei have recently become the subject of intense experimental and theoretical investigations. It has been suggested that nucleus-nucleus interactions provide a dense collision complex through compression and secondary particle production.[1] Evidence of collective flow has been reported in the low energy region ($\leq$ 1 GeV//nucleon).[2] At higher energies ($\leq$ 4 GeV/nucleon) it has been argued that a nucleus still exhibits a rather large stopping power.[3] If such a situation is realized, the formation of nuclear matter at high baryon density and at high temperature is expected[4] and transition to a new phase of hadronic matter such as Lee-Wick matter or quark-gluon plasma is predicted and is of great current interest in hadron dynamics.[5-7]

From another viewpoint, existing experimental data on particle production in high energy ($\leq$400 GeV) hadron-nucleus interactions are satisfactorily described in the framework of multiple scattering models as a superposition of independent elementary collisions of incident hadrons inside the target nucleus.[8,9] This suggests that the nucleus is a rather transparent object at high energies. It is necessary to investigate whether such an approach can be extended to nucleus-nucleus interactions.

Experimental testing of different hypotheses has not been possible at accelerators because high energy heavy ion beams are not yet available. This situation is expected to change in the next several years with the operation of new heavy-ion beams at CERN and BNL.[1] In the meantime, the cosmic rays provide a ready though sparse source of high energy heavy nuclei.

The balloon-borne counter-emulsion hybrid experiment was designed to study the collisions of heavy cosmic ray nuclei with different nuclear targets at energies above 20 GeV/nucleon. The electronic detectors, used to identify primary particles by energy and charge, allow selection of a set of interactions with minimum bias. The balloon-flight of the hybrid experiment was the fourth in a series of high energy cosmic ray experiments performed by the Japanese-American Cooperative Emulsion Experiment (JACEE) collaboration.[10,11]

In this paper we present the methods and results of exclusive analysis of the nucleus-nucleus interaction data and also inclusive treatment of this data set. In section 2, the instrumentation and experimental procedure are briefly described. In section 3, the experimental interaction cross-section for "Fe" ($22 \leq Z_p \leq 28$)-CHO (plastic) interactions is given, and multiplicities and pseudo-rapidity distributions for individual targets obtained from the inclusive data are compared with current models of nucleus-nucleus collisions.[9,12,13] The number distribution of participant projectile nucleons are compared with the Glauber calculation[14] for wounded nucleons for the "Fe"- CHO interactions. In section 4, we define a subset of the "Fe"- CHO collisions as "central" from the deduced number of wounded nucleons. Their cross-section is derived using the results of the number distribution of projectile participant nucleons and the value of the interaction cross-section for "Fe"- CHO collisions from section 3. The pseudo-rapidity distribution of the "central" "Fe"- CHO collision subset is compared with a calculation from the Multi-Chain Model.[13] In section 5, characteristics of the highest multiplicity events for individual targets are described. A non-uniform azimuthal distribution of produced particles for one of these events (with

a CHO target) is presented. Pseudo-rapidity distributions for the highest multiplicity events with emulsion and lead targets are compared with the Multi-Chain Model.

2. Description of Instrument

The instrument, shown schematically in Figure 1, consisted of electronic counters placed above an emulsion chamber. The details of the apparatus and counter performance have been described in the technical reports.[10] Electronic measurements of charge, energy and trajectory of incident particles were made with sufficient precision to allow unambiguous identification of the corresponding tracks in the plates of an emulsion chamber placed below. The energy of each nucleus was measured by a gas Cherenkov counter containing Freon-12 at atmospheric pressure, with an energy threshold of 20 GeV/nucleon. Differential energy measurements for iron-group nuclei were made from 20 to 65 GeV/nucleon with an accuracy of 10% at 55 GeV/nucleon. The charge determinations were made with two Cherenkov detectors employing flat sheets of lead glass and Teflon radiators. Both were in saturation in the energy region of interest (above 20 GeV/nucleon), where their first order response was therefore simply a function of the nuclear charge squared. Charge resolution was $\approx$ 1.1 units of charge (FWHM) in the charge and energy regions reported here. The multiwire proportional counter hodoscope, which consisted of 8 planes of wire chambers, determined the trajectories of incident particles. It gave the track location ($\sigma_{x,y} \leq 3.4$ mm) and incident angles ($\Delta\theta$, $\Delta\phi \leq 1.5^{o}$) which were then extrapolated into the emulsion chamber. The accidental probability of two iron group tracks ($Z_p \geq 22$) having the same coordinates within these errors was less

than 10^{-4} for the present experiment. To facilitate the tracing of tracks and to check for interactions above the emulsion chamber, several thin layers of passive materials (CR-39 and emulsion) were inserted just above and below the proportional counters.

The emulsion chamber used in this experiment was similar to that used in previous JACEE flights,[11] but was of area 50 cm x 50 cm to match the electronic counters. The emulsion chamber consisted of three modules: (1) the primary charge determination module at the top, 4.9 g/cm^2 thick, comprised a variety of emulsions and track recording CR-39 plastic; (2) the target module where interactions occur preferentially, 35.3 g/cm^2 thick, consisted of 121 emulsion plates, 11 CR-39 plates, 22 lead plates, and 66 acrylic plates placed periodically, and (3) the calorimeter module, 4 radiation lengths deep, which contained 11 layers each of lead, x-ray film, and emulsion. This chamber contained a larger than usual number of double-sided emulsion plates in the target module to facilitate secondary particle tracking in the central region of rapidity.

Primary nuclei measured by the electronic counters were initially located in the top layers of CR-39 plastic and the charges verified. Interaction vertices were then found by tracing down the stack using CR-39 plates placed every 10 layers. This procedure is sensitive to changes in nuclear charge of $\Delta Z > 2$ by etch-pit size measurement. Secondary particle tracks in emulsion plates just below the interaction were then used to locate the vertex. Tracing and measurement of polar and azimuthal angles of produced charged particles were made with a typical error in relative angle measurement of $<2 \times 10^{-4}$ radian, corresponding to errors of 0.01 and 0.2 for pseudo-rapidities in the central and fragmentation forward region, respectively.

Charges of fragment nuclei with $Z_f \geq 14$ were determined from CR-39 plates with a charge resolution of better than one unit of charge. For lighter fragments the δ-ray counting method ($4 \leq Z_f \leq 14$) and the grain counting method ($Z_f = 2,3$) were used with a charge resolution of 0.5 units of charge or better.

The hybrid detector was exposed to the cosmic rays for 39 hours on a balloon at an altitude of 5 g/cm^2 in June 1982. The number of high charge events ($Z_p \geq 22$) available for study was limited to 125 events by the cosmic ray flux, the geometric aperture of the instrument (0.16 m^{2}sr), and fragmentation in the atmosphere and instrument above the emulsion chamber.[10]

Figure 1.

3. Inclusive Characteristics

From 125 cosmic ray nuclei detected by the electronic counters with primary charge $Z_p = 22 - 28$ and energy greater than 20 GeV/nucleon, 105 interactions were found in the emulsion chamber. Among these interactions, 83 with energies in the range 20-65 GeV/nucleon were fully analyzed, i.e., the emission angles and charges of all charged particles emitted in the forward CMS hemisphere were measured. The remainder either had energies greater than 65 GeV/nucleon or their interaction vertices were too far (> 2 mm) above an emulsion layer to perform accurate measurements of all secondary tracks emitted in the forward cone. Table I summarizes the disposition of the 125 primaries, and the primary and target composition of the interactions.

Table I

From an analysis of interaction path lengths in the chamber for the 72 events with plastic (CHO) targets, an interaction cross section of 1.37 ± 0.16 barns was obtained. Here the atomic ratio of CHO and emulsion targets shown in Table I were used. The obtained value of the cross section for CHO targets is consistent with a recent Glauber model calculation, $\sigma_{Fe-C} = 1.76$ barns and $\sigma_{Fe-O} = 1.91$ barns at 2 GeV/nucleon[15] which leads to $\sigma_{Fe-CHO} = 1.26$ barns.

For each event we defined the "forward multiplicity" of produced singly charged particles in the collision of nucleus A on B, N_{mf}^{AB}, by the total charge $\Sigma|Z_i|$ measured within the half angle ($\theta \leq \theta_c$) less the charge of the projectile nucleus (Z_p). Here θ_c corresponds to $\pi/2$ in the center of mass of the nucleon-nucleon system ($\tan(\theta_c) = 2m/(2m(m+E_p))^{\frac{1}{2}}$), where m is the nucleon mass and E_p is primary energy per nucleon,

$$N_{mf}^{AB} = \Sigma|Z_i| - Z_p \quad . \tag{1}$$

In the backward hemisphere we had some bias for large angle track detection that depends on the position of the vertex with respect to the first measurable emulsion layer. Thus, the analysis performed in this paper is restricted to the particle production in the forward cone only. Since we could not identify individual singly charged particles, we assumed that protons released from the incident nucleus are emitted at smaller angles than produced particles (mostly mesons). This assumption allowed us to separate released protons from produced particles in the pseudo-rapidity variable.

In Figures 2(a), (b) and (c) the inclusive pseudo-rapidity distributions are shown for iron group nuclei interactions with different targets where the growth of the multiplicity with increasing target mass is illustrated. The solid curves in the figures are given for produced singly charged particles calculated from the Multi-Chain Model[13] (MCM) which is currently the only available model to predict pseudo-rapidity distributions.

Figures 2(a), (b), and (c)

Table II summarizes the inclusive data on the multiplicities N_{mf}^{AB} and the dispersions D of produced singly charged particles in the forward cone for interactions with different target nuclei. The values of the $D/\langle N_{mf}^{AB}\rangle$ ratio listed in the last column are close to unity irrespective of the target mass, and are more than twice as large as those observed in hadron-nucleus interactions. The large value of the dispersion of the multiplicity distribution in the nucleus-nucleus collisions compared to proton-nucleus collisions would be caused by the wider spread in the number of wounded nucleons due to the variation in impact parameters in such interactions. The experimental values obtained here on $D/\langle N_{mf}^{AB}\rangle$ are consistent with the predictions of different superposition models for nucleus-nucleus interactions[9,12,13] which give the $D/\langle N_{mf}^{AB}\rangle$ values between 0.9 and 1.3 depending on the model.

Table II

In Table III, the obtained mean forward multiplicities from this measurement are compared with the values calculated from the Wounded Nucleon Models (WNM1[12] and WNM2[9]) and the Multi-Chain Model[13] (MCM). Details of the use of these models are given in the Appendix.

Table III

The data are within two standard deviations of the calculated values. This comparison of the data with model calculations does not allow a conclusion as to which model is most favored.

Among the 83 events fully analyzed from this experiment, the set of 55 events with plastic (CHO) targets presents the best statistical sample for a comparison with model expectations. The number of participant projectile protons (which may or may not be 'wounded') is defined by

$$N_{part}\ (\text{protons}) = Z_p\ (\text{projectile charge}) - \Sigma Z_f\ (\text{heavy fragment charge})$$

$$- N_{sp}\ (\text{number of spectator protons}).$$

N_{sp} was defined in the present work for each event by consecutively adding all relativistic singly charged tracks, starting with the most forward track until the root mean square of the emission angles satisfies the evaporation formula of Goldhaber[16], $(<\theta^2_{lab}>)^{\frac{1}{2}} = 0.12/E_p$, (evaporation temperature was assumed to be 10 MeV).

In order to estimate the uncertainty in the determination of the number of spectator protons by this method, a Monte Carlo simulation was performed using the following assumptions: Goldhaber's formula was used

for emission angles of spectator protons; the differential function $\exp(-P_t/250\ \text{MeV/c})\ P_t dP_t$ was used for the transverse momentum (P_t) distribution of participant protons; in one or two successive collisions of participant protons a uniform distribution of inelasticity coefficient was assumed; production of baryon-antibaryon pairs was neglected; and pion contribution for laboratory pseudo-rapidities greater than 5 was assumed negligible. The simulation shows that the method of determining the spectator protons used here gives only a slightly greater average number (+0.05 to 0.8) than that used as input to the Monte Carlo simulation. With this confirmation, one can estimate the total number of participant nucleons by the formula:

$$N_{part} = (Z_p - \Sigma Z_f - N_{sp})A/Z_p \qquad (2)$$

Figure 3 shows the relationship of forward multiplicity $\langle N_{mf}^{AB} \rangle$ and the number of participant nucleons for "Fe"-CHO collisions. The observed correlation between the multiplicity of produced mesons and the number of participant nucleons is almost linear but much weaker than that expected from the simple superposition of proton-nucleus collision which is shown by the solid line in Figure 3. This difference may be explained if, among participant nucleons as defined here, there are nucleons which do not contribute efficiently to the particle production. Such might be elastically scattered nucleons and those involved in cascades.

Figure 3

In Figure 4 we display the observed distribution of the participant nucleon number from the "Fe"-CHO sample, determined by the method discussed above. The dashed curve in the figure gives the predicted distribution for wounded nucleons from the Glauber model.[14] As seen in this figure, the observed number of participant nucleons is significantly larger than the expected number of wounded nucleons from the Glauber calculation.

Figure 4

The previously mentioned experimental results from proton-nucleus collisions may be helpful in explaining this discrepancy. In hadron-nucleus collisions, the number of fast protons (30 MeV < E < 400 MeV) emitted from the target nucleus is known to be about twice as large as the number of proton-nucleon collisions of the primary proton inside the target nucleus.[9] This has been explained by assuming that recoil protons are rescattered inside the target nucleus,[17,18] which increases the number of fast protons, but not the multiplicity of produced particles in the final state. This model, if applicable for heavy ion collisions, would explain why the distribution of participant nucleons has a spread about twice as wide as that of the wounded nucleons. Although this plausible explanation fits the observations well, the real situation in nucleus-nucleus collisions may not be so simple. It is not clear whether every wounded nucleon in the projectile can produce recoil particles in the same manner as in proton-nucleus collisions, since they would be localized in the overlapping regions of projectile and target, where many neighboring nucleons are already wounded.

4. Central "Fe"-CHO Collisions

For the subsequent discussion an "Fe"-CHO "central collision" is operationally defined as having a total charge of spectators, $(\Sigma Z_f + N_{sp}) < 14$ corresponding to $N_{part} > 26$, where $N_{part} = 26$ is the maximum value in the Glauber calculation for ^{56}Fe-C. Eighteen of the 55 CHO target events were selected by this criterion. Figure 5 presents the composite pseudo-rapidity distributions of singly charged particles and fragments in the center of mass system for these "central collisions". The average observed multiplicity for central collisions may be compared with a multiplicity calculation under the superposition hypothesis. Based on the impact parameter picture and on the interaction cross-section of 1.37 ± 0.16 barns as mentioned in section 3, the cross-section of central collisions as defined above is 1.37(18/55) = 0.45 barns which corresponds to a geometrical cross-section of impact parameter less than 3.8 fm. The average number of wounded nucleons inside the iron projectile in this case is then estimated by the Glauber model calculation to be 15.7. Multiplying this number by $\langle N_{mf}^{p\text{-CHO}} (\eta > \eta_c) \rangle = 2.5$ (the average charged multiplicity[8]), we get $N_{mf}^{Fe\text{-CHO}} = 39$ which is in agreement with the observed value (34.3 ± 9.2).

Figure 5

The Multi-Chain Model,[13] which takes into account the deceleration of nucleons, gives a value of $N_{mf}^{Fe\text{-CHO}}$ of 35.5 for the central collisions, which is also consistent with the experimental value. Also, the prediction of the pseudo-rapidity distribution from the MCM is shown as the solid

curve in Figure 5 and is in good agreement with the data.

Recently, arguments about the stopping power of the nucleus have indicated that the deceleration of projectile hadrons is significant for central proton-nucleus collisions.[3] This effect would increase the significance of transverse to longitudinal motions and tend to increase the number of wounded nucleons and consequently the number of pions. As our knowledge of the details of this problem is presently limited, it is an open subject for future theoretical and experimental work.

5. The Highest Multiplicity Events

In the limited sample of heavy ion cosmic ray interaction studies, events with large produced-particle multiplicity have historically held special interest, partly because they signal central collisions and partly because individual events often have enough produced particles for statistically significant analysis.

In this section, characteristics of the highest multiplicity events observed in "Fe"-nucleus collisions are presented and discussed. As shown in Figure 3, the multiplicities in individual "Fe"-CHO interactions are widely spread and there are high multiplicity events separated by more than two standard deviations from the mean value. Such events also exist in "Fe"-Emulsion and "Fe"-Pb subsamples of interactions. To describe the characteristics of high multiplicity events we list in Table IV several features of the largest 25% of all interactions, ranked in order of decreasing multiplicity for each of the three target classifications.

Table IV

5.1 The Highest Multiplicity Event in Plastic Targets

Among the events listed in Table IV, the highest multiplicity "Fe"-CHO interaction is #6-869 with 121 observed singly charged particles for opening angle $\theta < \theta_c = 15^o$. The pseudo-rapidity and azimuthal angle distributions for this event are shown in Figure 6. This event has an obvious non-uniform azimuthal distribution of produced particles over the entire pseudo rapidity region. A χ^2 test for azimuthal uniformity showed the observed amount of anisotropy occurred in 5% of the cases if the particles were distributed randomly in azimuth. The azimuthal distribution is consistent with a dipole distribution at any rapidity region, and the pseudo-rapidity distribution does not exhibit an isotropic distribution. This azimuthal clustering of produced particles, suggests collective behavior,[2] but needs additional events for confirmation.

Figure 6

5.2 The Highest Multiplicity Events on AgBr and Pb Targets

Figures 7 (a) and (b) show the pseudo-rapidity distributions for the highest multiplicity events with Pb and emulsion targets, respectively. The azimuthal angle distributions of these events were consistent with isotropy. The pseudo-rapidity distributions show a significant central peak for these events. These figures include calculations of the rapidity distributions for produced singly charged particles from the Multi-Chain Model[13] using the measured projectile charge and energy from the electronic counters and assuming an impact parameter of b = 0 fm. As can be seen from the figure, the MCM model does not reproduce well the observed rapidity distribution for these events, especially in the central region. It is noted that one of these events (Ti - Pb, E_p = 42 GeV/nucleon) has a central rapidity density [$(dN/d\eta)_{max}$ = 97] as large as those observed in other previously reported events[19] at a much higher energy (above 1 TeV/nucleon).

Figure 7 (a) and (b)

6. Conclusions and Discussion

The inclusive data on the average multiplicity, its dispersion, pseudo-rapidity distributions and the average number of participant protons have been obtained for a limited sample of "Fe" - CH0, "Fe" -Emulsion, and "Fe" - Pb interactions at energies from 20 to 65 GeV/nucleon. The data are compared with proton-nucleus data and different super-position

models (WNM1[12], WNM2[9], MCM[13]). However, experimental errors and uncertainties in inputs to the model calculations do not allow a critical test of these models.

The average forward multiplicity increases approximately linearly with the number of participant nucleons, though the individual events are widely dispersed in this correlation. The observed numbers of participant nucleons are much larger than the expected number of wounded nucleons from a Glauber calculation.[14] Although this behavior might be inferred by comparison with the number of gray tracks in hadron-nucleus interactions, further investigation seems required on this point.

The pseudo-rapidity distribution of "Fe" - CHO central collision events is in agreement with that of the Multi-Chain Model in the central rapidity density. However, for the highest multiplicity interactions with heavy targets such as AgBr and Pb, the central rapidity density of the events exceeds the MCM predictions as seen in Figure 7.

In one of the highest multiplicity "Fe" - CHO events, an obvious dipole azimuthal distribution was observed, which may require a non-trivial explanation of structural flow of produced particles.

Both the pronounced central rapidity density and azimuthal structure observed in the highest multiplicity events are not readily understood by any of the existing superposition models.[9,12,13] It is an interesting question whether they are related to the postulated high baryon density states[4] or a quark gluon plasma phase transition.[5-7] Further observations of central collisions in this energy range (20-65 GeV/nucleon) is needed to confirm and understand these characteristics.

* This work was supported by the National Science Foundation, NASA and the U.S. Department of Energy in the USA, and by the Institute for Cosmic Ray Research, University of Tokyo, the Japan Society for the Promotion of Science, and the Kashima Foundation in Japan. We acknowledge the excellent support of the National Scientific Balloon Facility personnel, Palestine, Texas, in the successful balloon flight.

Appendix

In the model calculations there are some ambiguities in treating multiplicities of charged particles at lower energies due to the leading particle effect and charge exchanges. Here we briefly describe representations used in this paper.

Following the idea of the Wounded Nucleon Models (WNM)[9,12], the total charge in the forward hemisphere, $\Sigma|Zi|$ of equation (1) is presented for WNM1[12] as follows,

$$\Sigma|Z_i| = Z_p + \langle W_A^p \rangle \{\langle N_{\theta<\theta c}^{pp} \rangle (Z_T/B) + \langle N_{\theta<\theta c}^{pn} \rangle (1-Z_T/B)\}$$

$$+ \langle W_A^n \rangle \{\langle N_{\theta<\theta c}^{np} \rangle (Z_T/B) + \langle N_{\theta<\theta c}^{nn} \rangle (1-Z_T/B)\} \qquad (A-1)$$

where A and B are the mass numbers of projectile and target nuclei, respectively, $\langle W_A^p \rangle$ and $\langle W_A^n \rangle$ are the average numbers of wounded protons and neutrons, respectively, and $\langle N_{\theta<\theta c}^{ij} \rangle$ are the multiplicities of forward-produced singly-charged particles in nucleon-nucleon interactions, less leading charged particles. Superscripts denote nucleons in projectile (i) and target (j) nuclei, where p denotes proton and n neutron. Z_T is the charge of the target nucleus.

Assuming

$$\langle W_A^p \rangle = \langle W_A \rangle (Z_p/A), \quad \langle W_A^n \rangle = \langle W_A \rangle (1 - Z_p/A),$$

$$\text{and } \langle N_{\theta<\theta c}^{pp} \rangle = \langle N_{\theta<\theta c}^{pn} \rangle = \langle N_{\theta<\theta c}^{np} \rangle = \langle N_{\theta<\theta c}^{nn} \rangle$$

we obtain from the equation (A-1) the multiplicity of forward produced singly charged particles $\langle N_{mf}^{AB} \rangle$ for the case of WNM1 as follows,

$$\langle N_{mf}^{AB} \rangle = \Sigma |Z_i| - Z_p = \langle W_A \rangle \langle N_{\theta<\theta c}^{PP} \rangle \qquad (A\text{-}2)$$

$\langle N_{mf}^{AB} \rangle$ for the case of WNM2[9] is given in the same equation (A-1) by simply replacing $\langle N_{\theta<\theta c}^{ij} \rangle$ with the multiplicity of the forward-produced singly-charged particles less leading charged particles in the nucleon-nucleus interactions $\langle N_{\theta<\theta c}^{iB} \rangle$,

$$\langle N_{mf}^{AB} \rangle = \Sigma |Z_i| - Z_p = \langle W_A \rangle \langle N_{\theta<\theta c}^{pB} \rangle \qquad (A\text{-}3)$$

In these equations, the average number of wounded nucleons $\langle W_A \rangle$ was calculated by using the Glauber relation $\langle W_A \rangle = A\sigma_{pB}/\sigma_{AB}$. Here, the formula $\sigma_{pB} = (0.032 \sim 0.044)B^{(0.78 \sim 0.70)}$ barns[20,21,22] was taken as the proton-nucleus interaction cross section and the empirical formula $\sigma_{AB} = 0.078\ (A^{1/3} + B^{1/3} - 1.25)^2$ barns[23] was used as the nucleus-nucleus interaction cross section. The multiplicities of forward produced particles $N_{\theta<\theta c}^{PP}$ were interpolated from Morrison's data[24] at and Elias' data at 50 and 100 GeV, and $N_{\theta<\theta c}^{pB}$ were also obtained from Elias' data. For the mixed targets such as CHO and emulsion, the effective mean values were calculated using the number density of each constituent element as weights.

For the case of the Multi-Chain Model, produced multiplicities are directly calculated,

$$\langle N_{mf}^{AB} \rangle = \Sigma |Z_i| - Z_p = N^{MCM}\ (\theta<\theta_c) \qquad (A\text{-}4)$$

where N^{MCM} is the multiplicity of forward produced singly charged particles.[13]

REFERENCES

1. T. Ludlam and H. Wegner (Eds.), Proceedings of Quark Matter '83, Nucl. Phys. A418, 1, (1984).

2. H. A. Gustafson et al., Phys. Rev. Lett. 52, 1950, (1984).

3. W. Busza and A. S. Goldhaber, Nucl. Phys. A419, 635c, (1984).

4. S. Date, M. Gyulassy and H. Sumiyoshi, preprint NSS-Rep. 535, (1985).

5. H. Satz (Ed.), Statistical Mechanics of Quark and Hadron, North Holland, (1981).

6. E. V. Shuryak, Phys. Rev. C 61, 71, 1981 and ibid., C 115, 151, (1984).
   J. D. Bjorken, Phys. Rev. D 27, 140, (1983).
   J. Cleymans et al., Z. Phys., C 17, 341, (1983).

7. T. D. Lee and G. C. Wick, Phys. Rev. D 9, 2291, (1974).

8. J. E. Elias et al., Phys. Rev. D 22, 12, (1980).

9. I. Otterlund, Nucl. Phys. A418, 87c, (1984).

10. JACEE Collaboration, T. H. Burnett et al., Proceedings of the 19th International Cosmic Ray Conference, Bangalore, 9,375, (1983) and ibid., 9,379, (1983).
19th International Cosmic Ray Conference, La Jolla, 6,152, (1985), ibid., 6,156, 1985 and ibid., 6,160, (1985).

11. JACEE Collaboration, T. H. Burnett et al., Phys. Rev. Letters, 51, 1010, (1983).

12. A. Bialas, M. Bleszynski and W. Czyz, Nucl. Phys. B111, 461, (1976).
A Dar and J. Vary, Phys. Rev., D6, 2412, (1972).

13. K. Kinoshita, A. Minaka and H. Sumiyoshi, Z. Phys. C8, 205, (1981).

14. R. J. Glauber, Lectures in Theoretical Physics, edited by W. B. Britton et al., Wiley-Interscience, NY, 1, 315 (1959).
R. J. Glauber and G. Matthiae, Nucl. Phys., B21, 135, (1970).

15. H. Sato and Y. Okuhara, INS (Institute for Nuclear Study, University of Tokyo)-Rep.-558, (1979).

16. A. S. Goldhaber, Phys. Letters, 53B, 306, (1974).

17. M. K. Hegab and J. Hufner, Nucl. Phys. B198, 407, (1982).

18. N. Suzuki, Nucl. Phys. A403, 553, (1983).

19. JACEE Collaboration, T. H. Burnett et al., Phys. Rev. Letters, 50, 2062, (1983), and Proceedings of the "Quark Matter '84" Conference, Springer Verlag, 221, 187, (1985).

20. A. S. Carroll et al., Phys. Lett. 80B, 319, (1979).

21. S. P. Denisov et al., Nucl. Phys. B61, 62, (1973).

22. F. Fumuro, R. Ihara and T. Ogata, Nucl. Phys. B152, 376, (1979).

23. J. Jaros et al., Phys. Rev. C 18, 2273, (1978).

24. J. Whitmore, Phys. Reports, 10, 273, (1974); D. R. O. Morrison, CERN/D.Ph.IL/PHYS 73-46, (1973).

Figure 1. Schematic diagram of the hybrid counter-emulsion chamber instrument. The instrument comprised electronic counters (Freon-12 gas Cherenkov counter, lead glass and Teflon Cherenkov counters and multiwire proportional counter hodoscope) placed above an emulsion chamber and a scintillation counter placed below the emulsion chamber.

Figure 2. Inclusive pseudo-rapidity distributions of produced particles for different targets. 2(a) CHO target, 2(b) emulsion targets and 2(c) lead targets. The solid curve is the pseudo-rapidity distribution calculated from the MCM for produced singly charged particles.

Figure 3. The relation between forward singly charged multiplicity N_{mf}^{AB} and the number of participant nucleons for "Fe"-CHO collisions.

Figure 4. The distribution of the number of participant nucleons for "Fe"-CHO collisions. The histogram is the data from 55 interactions. The dashed curve indicates the expectation for wounded nucleons from the Glauber model.

Figure 5. The pseudo-rapidity distribution for "Fe"-CHO "central collisions". The composite pseudo-rapidity distribution of singly charged particles and fragments is indicated in the center of mass system at average energy 34.2 ± 9.1 GeV/nucleon for 18 central collisions ($N_{part} > 26$). The solid curve is the result of a MCM calculation for an impact parameter $b \leq 3.8$ fm. The spectator protons (N_{sp}) from the observations are to the right of the step-shaped solid line ending at $\eta - \eta_c = 4$.

Figure 6. The pseudo-rapidity and azimuthal angle distributions for the highest multiplicity Fe-CHO collision (#6-869).

Figure 7. Pseudo-rapidity distributions for the highest multiplicity events on emulsion and lead targets, (a): Ti - AgBr (#7-749) and (b): Ti - Pb(#7-642). The solid curves are calculated using the MCM with impact parameter b = 0 fm.

Table I. A summary of the tracing of the 125 primary particles with primary and target composition for 105 interactions.

Table II. Inclusive data on multiplicities and dispersions of produced singly charged particles in the forward hemisphere in the center of mass system. The data is grouped according to target.

Table III. Comparison between the experimental multiplicities and those calculated from simple superposition models (WNM1, WNM2 and MCM). Calculations were made for ^{56}Fe, while the data are "iron-group" (see Table I). For critical comparisons with data, calculated values must be reduced according to Table I.

Table IV. The upper 25% in multiplicity of all events for the three targets.

Table I

Number of Primary Nuclei from Electronic Counters ($Z_p \geq 22$, $E_p \geq 20$ GeV/nucleon)		125	
Nuclei Passed Through Emulsion Chamber		7	
Nuclei Interacted above Chamber		13	
Number of Nuclei that Interacted in Emulsion Chamber (9 Ti, 6 V, 12 Cr, 12 Mn, 65 Fe, 1 Ni)		105	
	(Target) CHO	Em	Pb
Number of Events in Emulsion Chamber	72	16	17
Events Having Energies $\geq$ 65 GeV/nucleon	14	2	1
Events that Interacted $\geq$ 2 mm above an Emulsion Layer	3	0	2
Number of Fully Analyzed Events ($E_p \leq$ 65 GeV/nucleon)	55	14	14
Composition of CHO:	33% C, 53% H, 14% O		
Composition of Emulsion	17.5% C, 40.7% H, 4.0% N, 12.0% O, 0.17% S, 12.7% Br, 12.8% Ag, 0.07% I		

Table II

Target	No. of Events	$\langle Z_p \rangle$	$\langle E_p \rangle$ GeV/nucleon	$\langle N_{mf}^{AB} \rangle$	$D/\langle N_{mf}^{AB} \rangle$
Plastic (CHO)	55	25.4±1.1	37.2±5.0	19.7±2.7	1.03±0.14
Emulsion	14	23.9±1.6	33.3±8.9	27.3±7.3	1.14±0.31
Pb	14	25.1±1.6	34.5±9.2	41.6±11.1	1.01±0.27

Table III

A - B	$\langle E_p \rangle$ GeV/nucleon	$\langle N_{mf}^{AB} \rangle$ WNM1	$\langle N_{mf}^{AB} \rangle$ WNM2	$\langle N_{mf}^{AB} \rangle$ MCM	$\langle N_{mf}^{AB} \rangle$ this work
"Fe" - CHO	37.2 ± 5.0	10∿14	14∿16	13	19.7 ± 2.7
"Fe" - Em	33.3 ± 8.9	17∿22	29∿32	20	27.3 ± 7.3
"Fe" - Pb	34.5 ± 9.2	31∿43	49∿57	33	41.6 ± 11.1

Table IV

Event #	E_p	Z_p	Interaction Mode (observed)	N_{mf}	N_{part}	$(dN/d\eta)_{o<\eta-\eta c<1}$
			<CHO Target>			
6-869	54	Fe	3He + 128 ch.	101	37	45
1-1214	39	Mn	He + 105 ch.	64	48	35
7-1598	40	Fe	1He + 96 ch.	57	39	28
5-1835	42	V	2He + 88 ch.	54	35	35
6-1596	45	Fe	2He + 90 ch.	52	37	25
6-1114	36	Ti	1He + 72 ch.	50	28	10
2-191	42	Fe	5He + 91 ch.	49	26	25
5-1215	23	Fe	1He + 75 ch.	39	43	18
6-1409	50	Fe	0 + 2He + 59 ch.	36	13	21
1-878	48	Fe	Sc + 2He + 54 ch.	36	2	17
7-1689	54	Fe	N + Li + 1He + 56 ch.	35	17	15
6-733	30	Fe	Li + 2He + 62 ch	35	30	23
5-607	23	Fe	B + 1He + 57 ch.	34	28	25
6-141	23	Fe	3He + 62 ch.	33	41	22
4-876	35	Fe	Be + 66 ch.	33	34	15
			<Emulsion Target>			
4-749	28	Ti	265 ch.	124	46	91
1-1047	63	Fe	4He + 97 ch.	51	24	25
7-148	48	Fe	Be + 2He + 62 ch.	41	26	23
8-1063	25	Mn	Si + 1He + 77 ch.	38	11	26
1-1004	28	Fe	C + 1He + 70 ch.	38	26	23
			<Pb Target>			
7-642	42	Ti	267 ch.	133	48	97
8-378	38	Mn	160 ch.	99	53	75
1-1542	48	Fe	1He + 145 ch.	97	43	51
6-1927	25	Fe	163 ch.	81	56	56

E_p in GeV/nucleon.

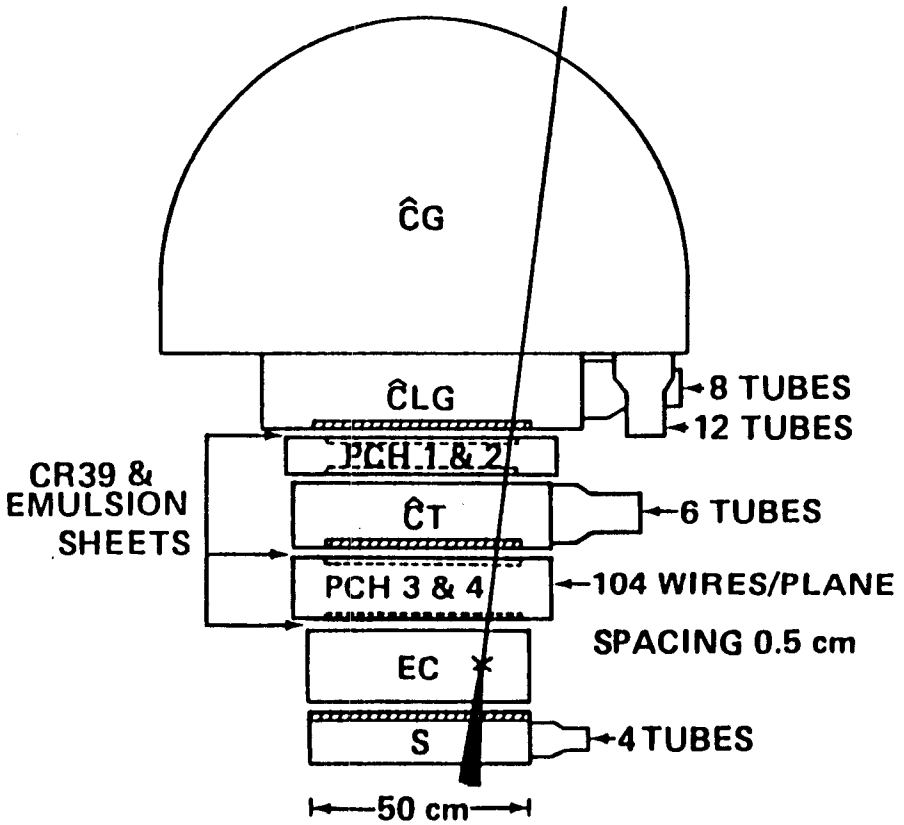

ĈG	–	GAS ĈERENKOV F12, 1 ATMOSPHERE
ĈLG	–	LEAD GLASS ĈERENKOV
ĈT	–	TEFLON ĈERENKOV
EC	–	EMULSION CHAMBER
S	–	SCINTILLATOR
PCH	–	PROPORTIONAL COUNTER HODOSCOPE

FIG 1

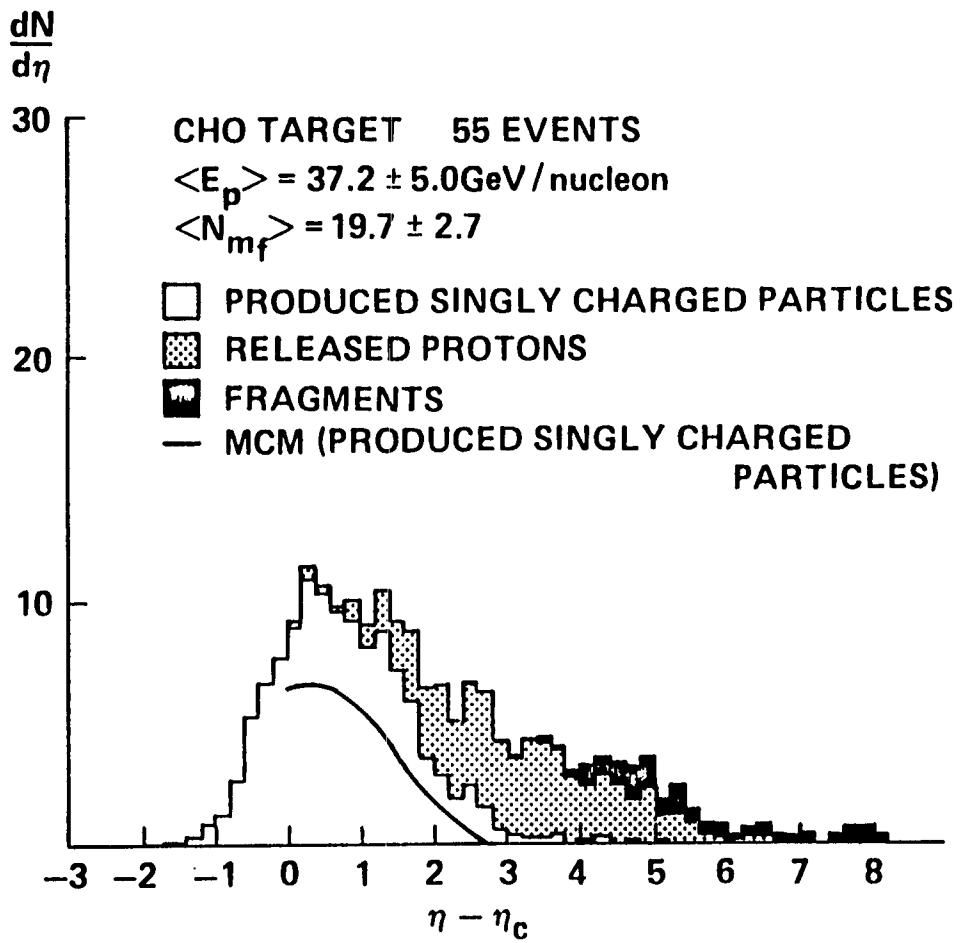
dN/dη
30
20
10
CHO TARGET 55 EVENTS
<E_p> = 37.2 ± 5.0GeV / nucleon
<N_mf> = 19.7 ± 2.7
PRODUCED SINGLY CHARGED PARTICLES
RELEASED PROTONS
FRAGMENTS
MCM (PRODUCED SINGLY CHARGED PARTICLES)
−3 −2 −1 0 1 2 3 4 5 6 7 8
η − η_c

FIG. 2a

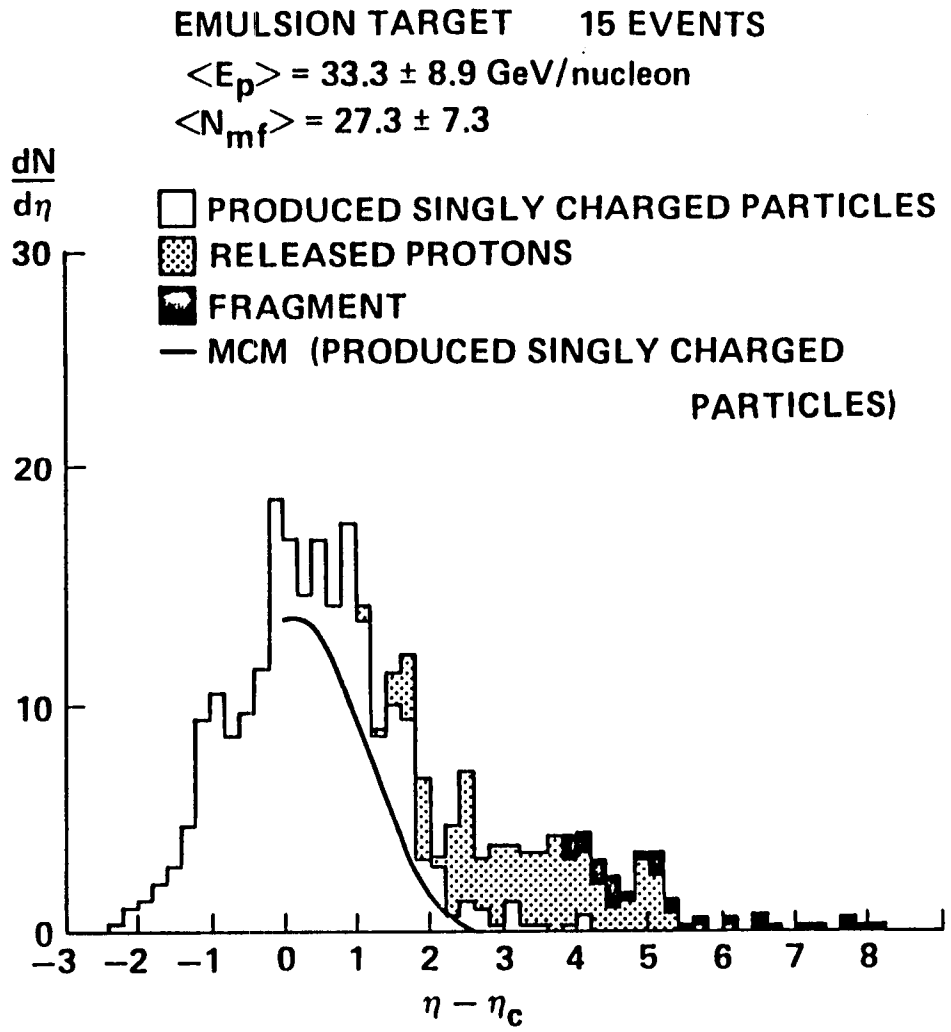
EMULSION TARGET 15 EVENTS
<Ep> = 33.3 ± 8.9 GeV/nucleon
<Nmf> = 27.3 ± 7.3
dN/dη
PRODUCED SINGLY CHARGED PARTICLES
RELEASED PROTONS
FRAGMENT
MCM (PRODUCED SINGLY CHARGED PARTICLES)
30
20
10
0
−3 −2 −1 0 1 2 3 4 5 6 7 8
η − ηc

FIG. 2b

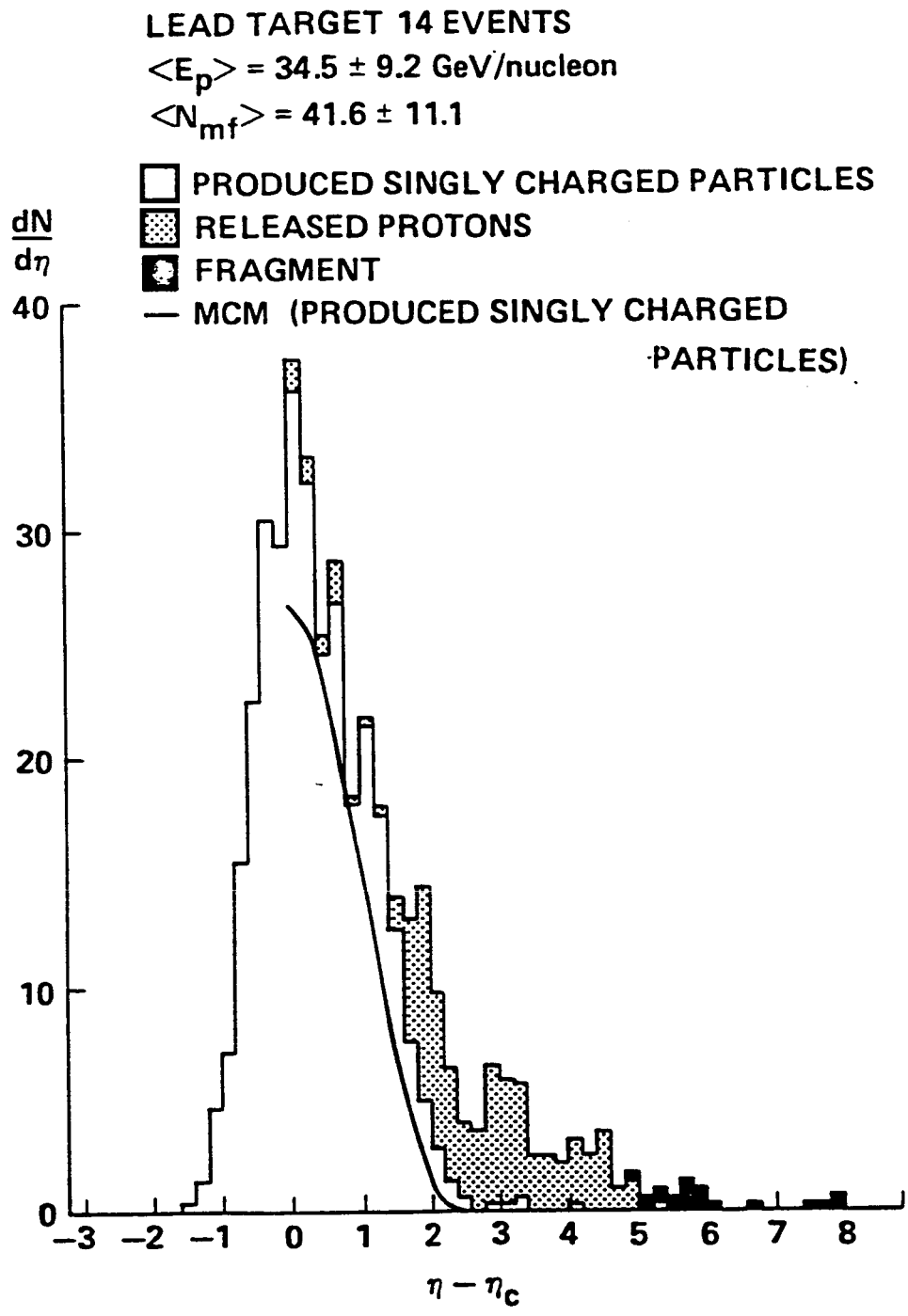
LEAD TARGET 14 EVENTS
<E_p> = 34.5 ± 9.2 GeV/nucleon
<N_{mf}> = 41.6 ± 11.1
PRODUCED SINGLY CHARGED PARTICLES
RELEASED PROTONS
FRAGMENT
MCM (PRODUCED SINGLY CHARGED PARTICLES)
dN/dη
40
30
20
10
0
−3 −2 −1 0 1 2 3 4 5 6 7 8
η − η_c

FIG. 2C

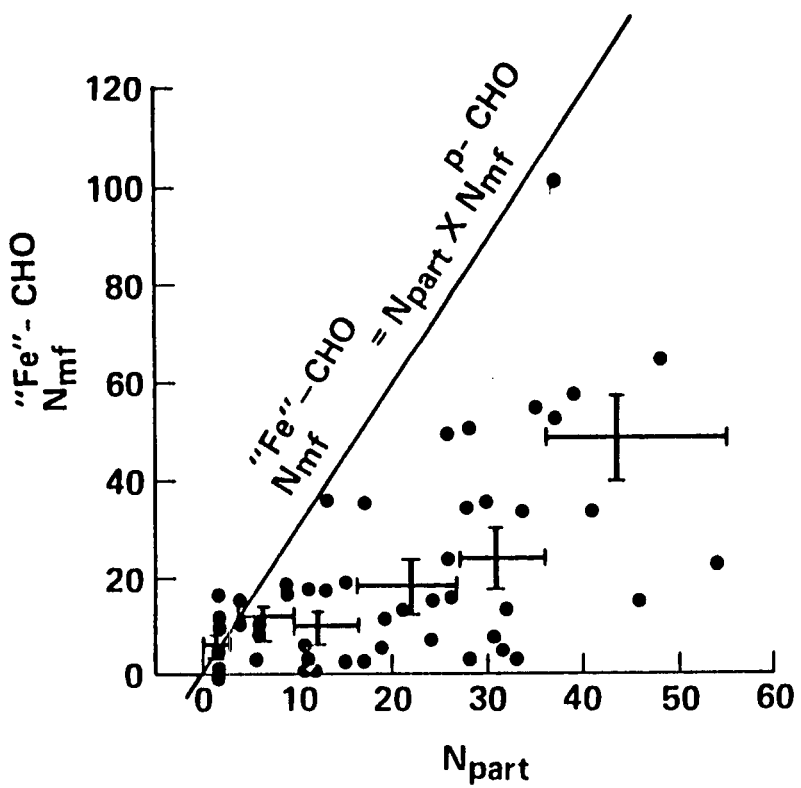
120
100
80
60
40
20
0
0
10
20
30
40
50
60
"Fe"- CHO
N_{mf}
N_{part}
"Fe"–CHO
N_{mf}
= N_{part} X N_{mf}^{p-CHO}

FIG. 3

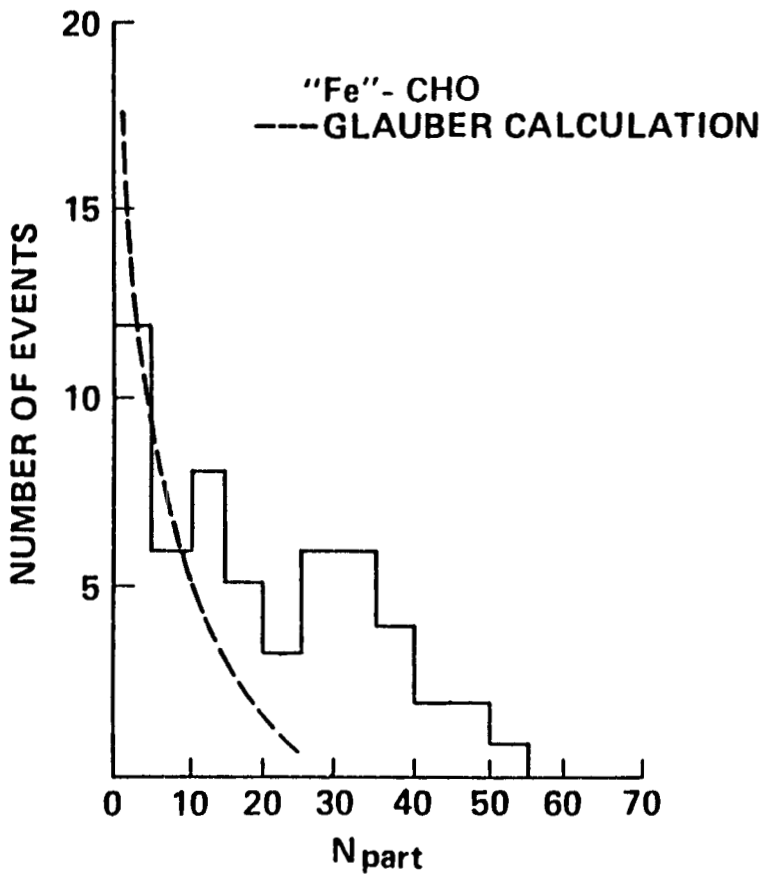
20
15
10
5
NUMBER OF EVENTS
"Fe"- CHO
---GLAUBER CALCULATION
0
10
20
30
40
50
60
70
N part

FIG. 4

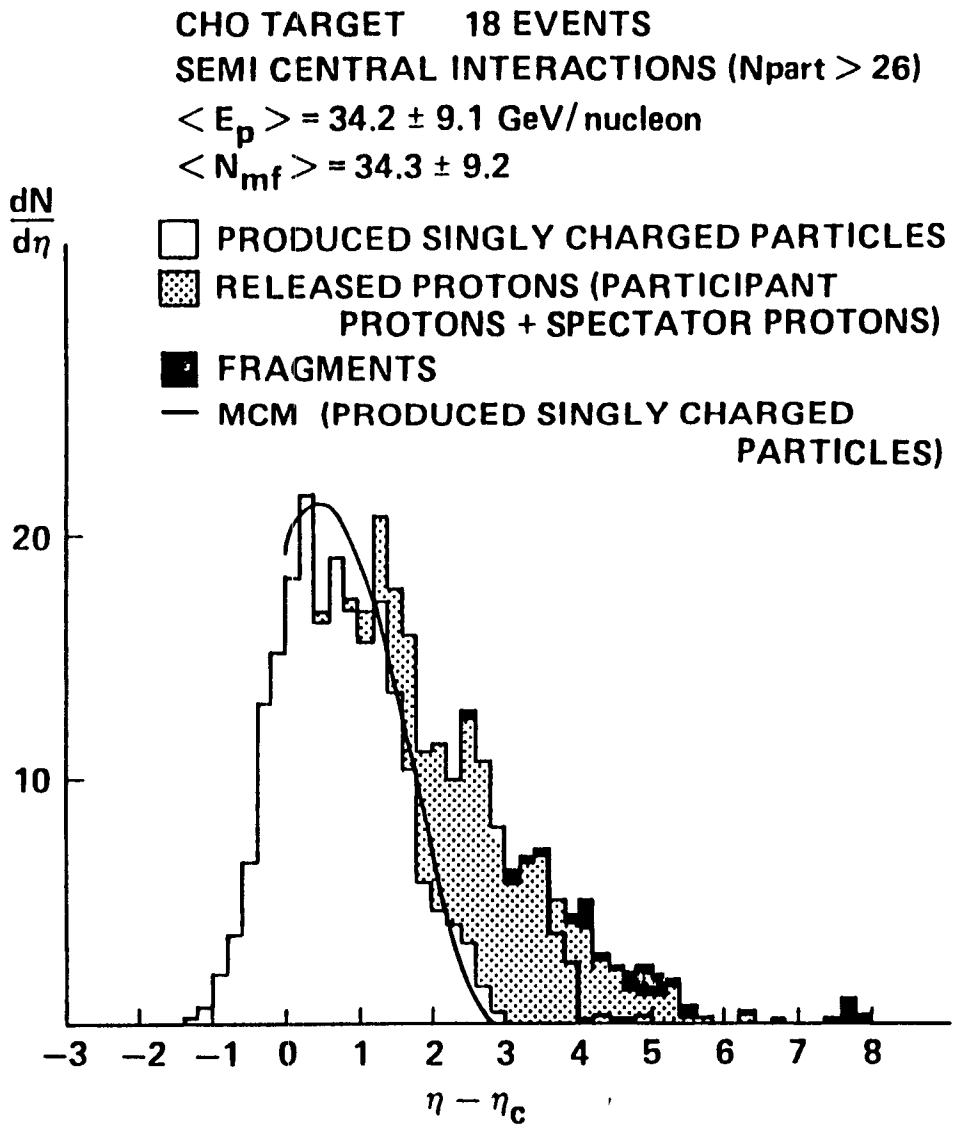
CHO TARGET 18 EVENTS
SEMI CENTRAL INTERACTIONS (Npart > 26)
< E_p > = 34.2 ± 9.1 GeV/nucleon
< N_{mf} > = 34.3 ± 9.2
dN/dη
PRODUCED SINGLY CHARGED PARTICLES
RELEASED PROTONS (PARTICIPANT PROTONS + SPECTATOR PROTONS)
FRAGMENTS
MCM (PRODUCED SINGLY CHARGED PARTICLES)
20
10
−3 −2 −1 0 1 2 3 4 5 6 7 8
η − $η_c$

FIG. 5

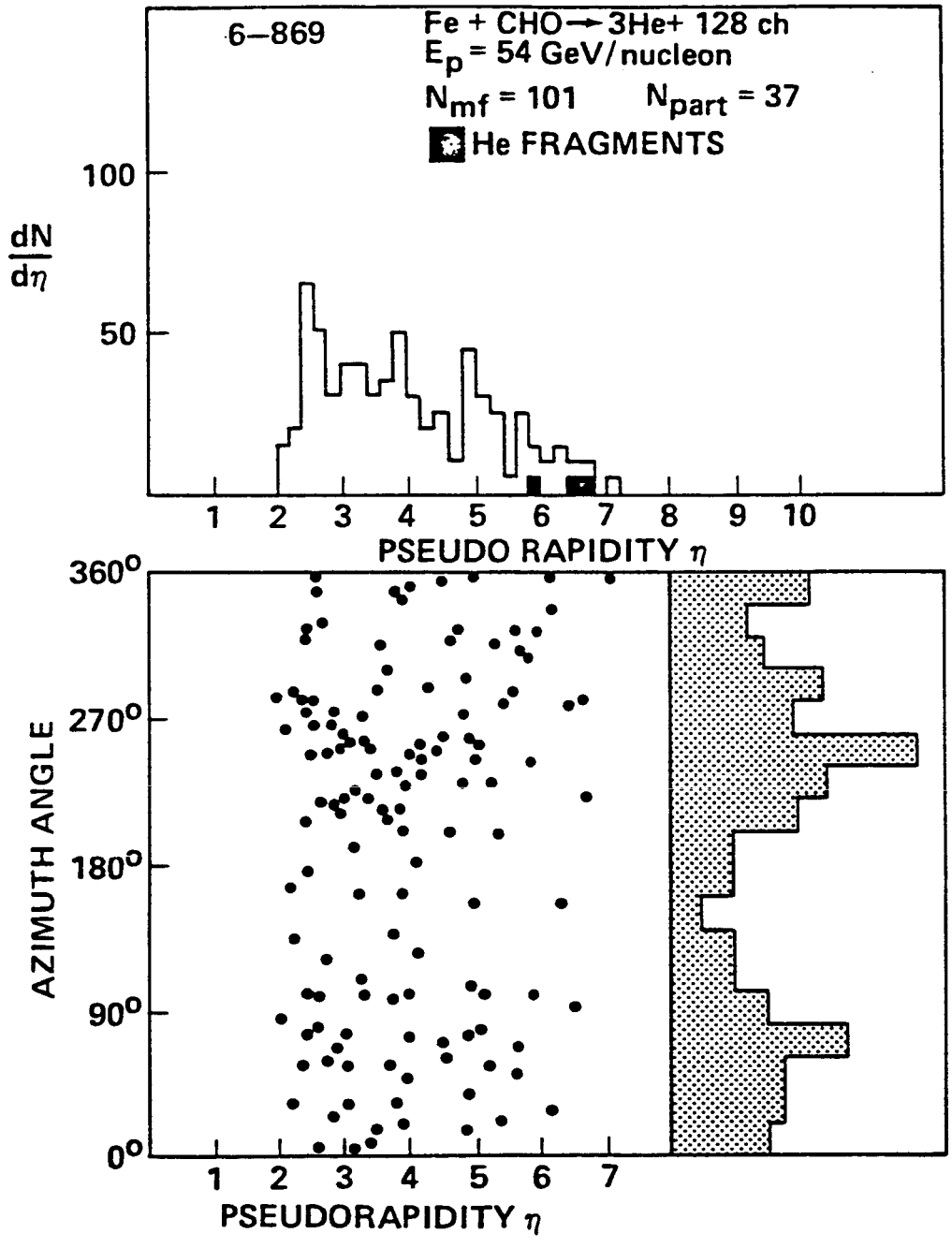
6–869
Fe + CHO → 3He+ 128 ch
E_p = 54 GeV/nucleon
N_{mf} = 101
N_{part} = 37
He FRAGMENTS
100
50
dN/dη
1 2 3 4 5 6 7 8 9 10
PSEUDO RAPIDITY η
360°
270°
180°
90°
0°
AZIMUTH ANGLE
1 2 3 4 5 6 7
PSEUDORAPIDITY η

FIG. 6

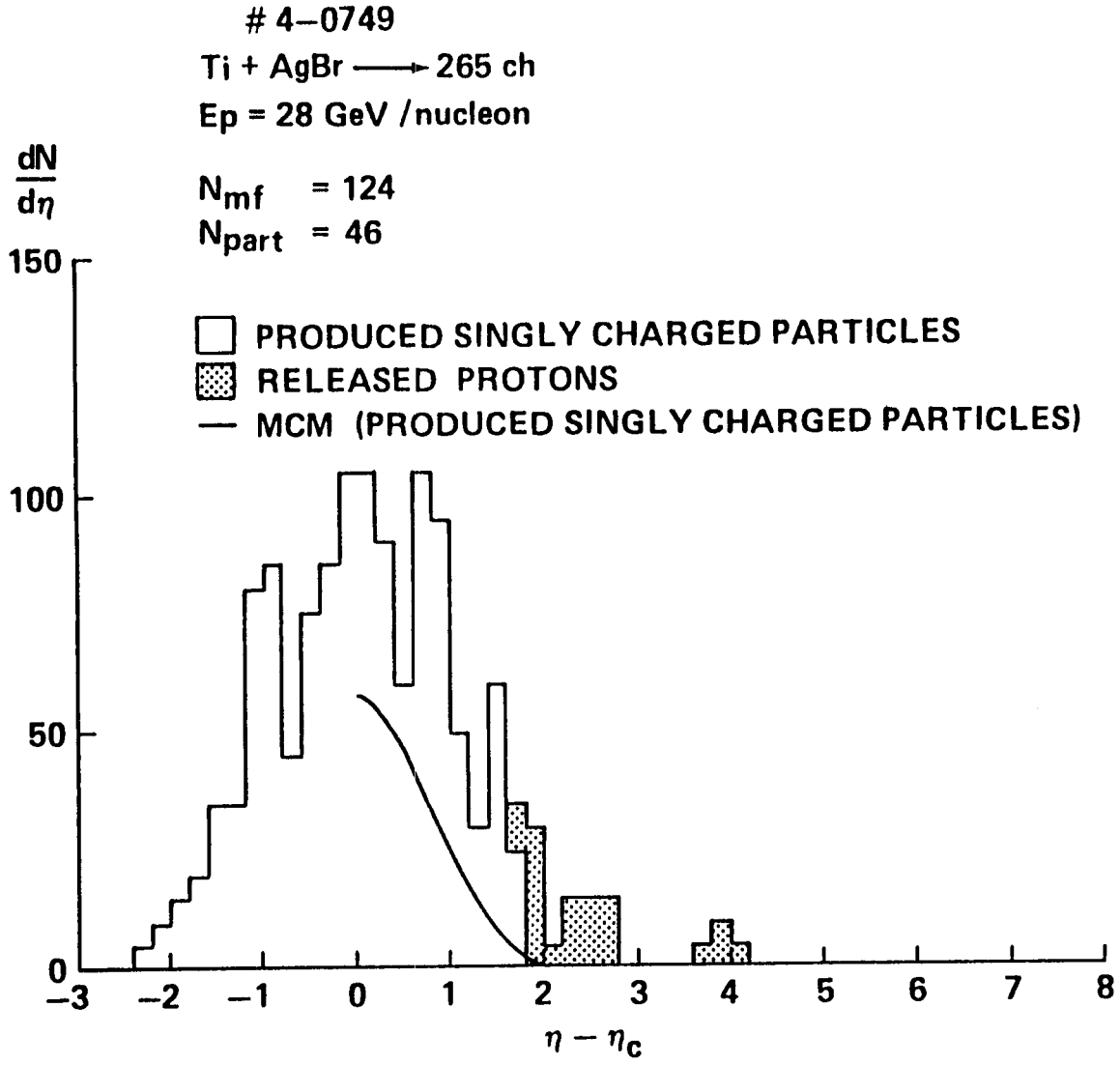
4–0749
Ti + AgBr ⟶ 265 ch
Ep = 28 GeV /nucleon
dN/dη
N_mf = 124
N_part = 46
PRODUCED SINGLY CHARGED PARTICLES
RELEASED PROTONS
MCM (PRODUCED SINGLY CHARGED PARTICLES)
150
100
50
0
−3
−2
−1
0
1
2
3
4
5
6
7
8
η − η_c

FIG. 7a.

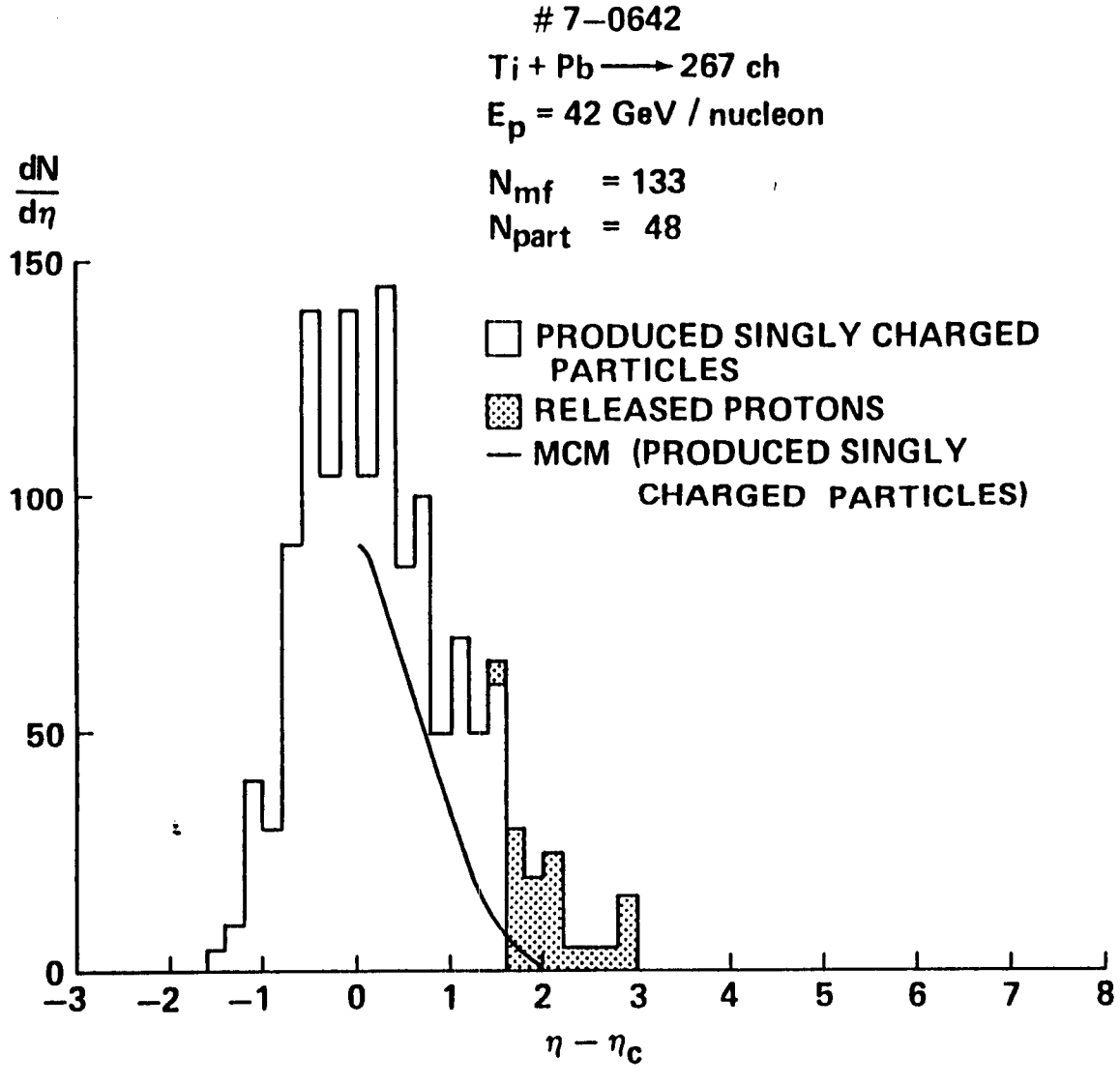
7–0642
Ti + Pb ⟶ 267 ch
E_p = 42 GeV / nucleon
N_{mf} = 133
N_{part} = 48
$\frac{dN}{d\eta}$
150
100
50
0
PRODUCED SINGLY CHARGED PARTICLES
RELEASED PROTONS
MCM (PRODUCED SINGLY CHARGED PARTICLES)
−3 −2 −1 0 1 2 3 4 5 6 7 8
$\eta - \eta_c$

FIG. 7b